

# Low-temperature thermochronology and its geological significance in the central-northern section of the western margin of the Ordos Basin

Guangyuan Xing<sup>1,2</sup>, Zhanli Ren<sup>1,2\*</sup>, Kai Qi<sup>1,2</sup>, Sasa Guo<sup>1,2</sup>, Yanzhao Liu<sup>1,2</sup>,  
Ying Zhang<sup>3</sup>, Huaping Lan<sup>4</sup>

<sup>1</sup> Department of Geology, Northwest University, Xi'an 710069, China;

<sup>2</sup> State Key Laboratory of Continental Evolution and Early Life, Xi'an 710069, China;

<sup>3</sup> Research Institute of Yanchang Petroleum(Group) Co.Ltd., Xi'an 710075, China;

<sup>4</sup> Research Institute No. 203 of Nuclear Industry, Xi'an 710000, China

Correspondence to: Zhanli Ren

E-mail: renzhanl@nwu.edu.cn

**Abstract:** The study of low-temperature thermochronology at plate edges provides favorable constraints for regional tectonic evolution and surface processes. Based on the existing thermochronological data of multiple cooling events since the Mesozoic era, we conducted apatite fission-track and apatite (U-Th)/He studies on drilling samples from the central-northern section of the western margin of the Ordos Basin, revealing the exhumation, cooling history and differences in the study area. The new thermal history simulation results show that the Zhuozishan Mountain (Mt.) region (ZM region) experienced large-scale exhumation in the Late Jurassic (160 Ma-150 Ma), with an average exhumation rate of ca. 45 m/Ma and an average cooling rate of ca. 2 °C /Ma, slow exhumation at Early Cretaceous - Oligocene (130 Ma-30 Ma), with an average exhumation rate of ca. 10 m/Ma and an average cooling rate of ca. 1 °C /Ma, and severe exhumation after Oligocene (30 Ma-present), with an average exhumation rate of ca. 30 m/Ma and an

27 average cooling rate of ca. 1.2 °C/Ma; The Taole - Hengshanbao region  
28 (TH region) began to exhumation at Late Jurassic - Early Cretaceous (155  
29 Ma-145 Ma), with an average exhumation rate of ca. 48 m/Ma and an  
30 average cooling rate of ca. 2.4 °C /Ma, slowly exhumation at Early  
31 Cretaceous - Oligocene (145 Ma-30 Ma), with an average exhumation  
32 rate of ca. 7.5 m/Ma and an average cooling rate of ca. 0.3 °C/Ma, and  
33 then violently exhumation, with an average exhumation rate of ca. 25  
34 m/Ma and an average cooling rate of ca. 1 °C /Ma; The Majiatan -  
35 Huianbao region (MH region) experienced large-scale exhumation at Late  
36 Jurassic - Early Cretaceous (158 Ma-137 Ma), with an average  
37 exhumation rate of ca. 45 m/Ma and an average cooling rate of ca. 1.8 °C  
38 /Ma, with a slightly slower exhumation rate at 137 Ma-110 Ma, with an  
39 average exhumation rate of ca. 13 m/Ma and an average cooling rate of ca.  
40 0.52 °C /Ma, and entered a severe exhumation stage again at Late  
41 Cretaceous - Eocene (70 Ma-50 Ma), with an average exhumation rate of  
42 ca. 37.5 m/Ma and an average cooling rate of ca. 1.5 °C/Ma. The Late  
43 Jurassic tectonic exhumation indicated by thermochronology corresponds  
44 to the formation of the western margin thrust fold structure, with the  
45 northern and southern sections starting earlier and the central section  
46 starting slightly later. At the same time, the exhumation time of different  
47 fault blocks decreases gradually from the edge of the basin to the interior  
48 of the basin, in the east-west direction. This is related to the different

49 tectonic evolution and stress in their location.

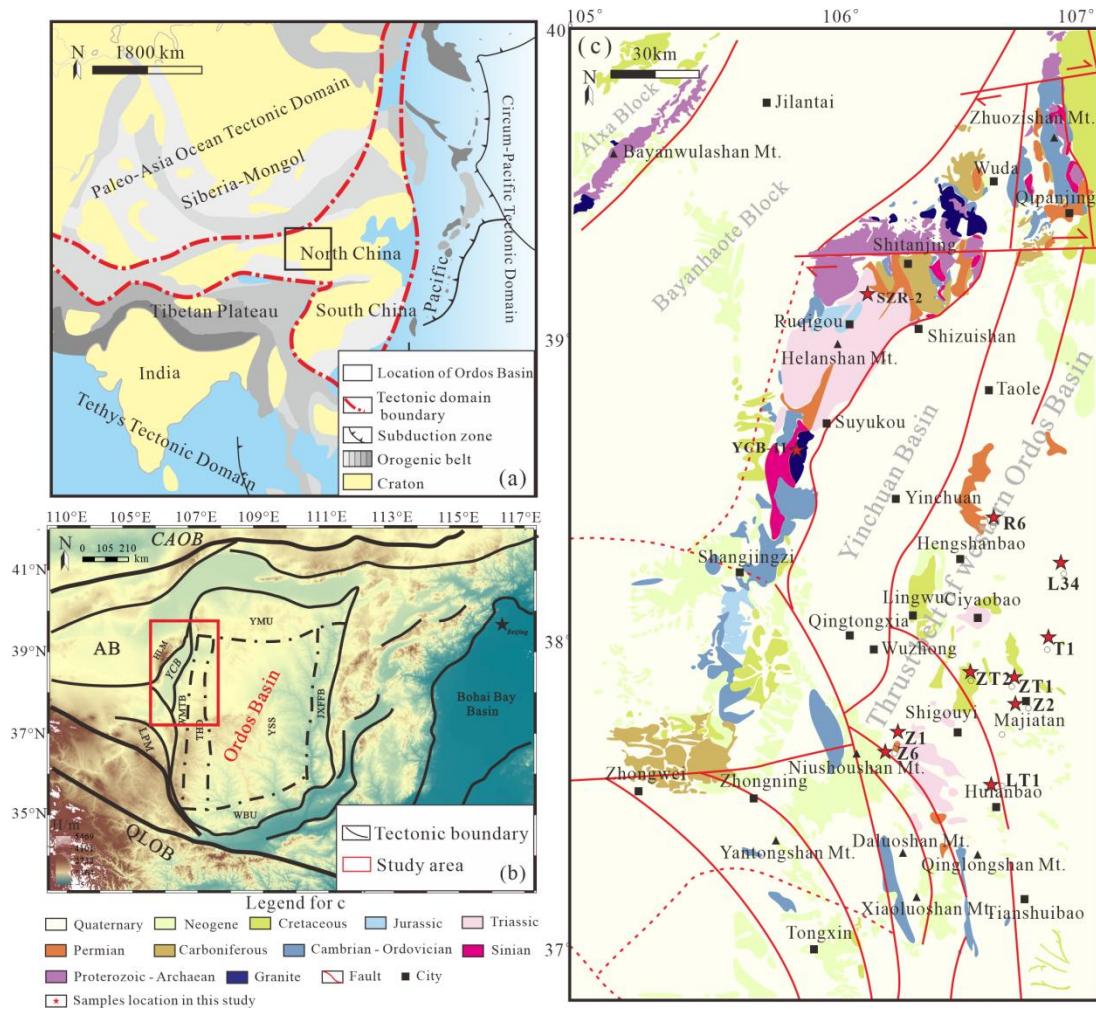
50 **Keyword:** Ordos Basin; North China Block; Plate convergence;

51 Low-temperature thermochronology; Yanshanian orogeny

## 52 **1 Introduction**

53 The North China Craton, as one of the oldest cratons in the world,  
54 has a long history spanning 3.8 billion years (Zhai, 2010; Zhang et al.,  
55 2018). Having undergone prolonged and complex tectonic evolution, it  
56 records nearly all major tectonic events from ancient to the present,  
57 especially preserving multi-phase evolutionary remnants since 1.8 Ga  
58 years (Peng et al., 2022). The Ordos Block is part of the North China  
59 Craton and one of its core geological units (Bao et al., 2019; Zhai, 2021).  
60 The present-day Ordos Basin, in a narrow sense, is located in the western  
61 part of the North China Craton, and has been developed since the  
62 Mesozoic as a residual intra-cratonic basin (Ren, 1995; Zhai, 2021). This  
63 basin is superimposed on a large Paleozoic basin, making it a composite  
64 basin (Liu et al., 2005). The Ordos Basin preserves the most complete  
65 sedimentary strata in North China Craton, including the Archaean,  
66 Proterozoic, Paleozoic, Mesozoic, and Cenozoic strata, and is rich in  
67 various energy and mineral resources such as oil, gas, coal, and uranium  
68 deposits. The thrust belt along the western margin of the Ordos Basin  
69 spans between tectonic blocks with different characteristics, including the  
70 North China Craton, the Alxa Block, the Central Asian Orogenic Belt, the

71 Qinling Orogenic Belt, and the northeastern edge of the Tibetan Plateau  
 72 (Fig.1). It is one of the regions with the most intense tectonic deformation  
 73 within the Chinese mainland since the Mesozoic, recording numerous  
 74 intracontinental deformation and orogenic events since the Mesozoic.



75 Fig.1 (a) Tectonic setting of China (modified from Peng et al., 2019), (b) Digital  
 76 elevation model of the Ordos basin and surrounding areas. The red rectangle is the  
 77 research area of this article (modified from Qi et al., 2024), abbreviation: AB, Alxa  
 78 Block; CAOB, Central Asian Orogen Belt; HLM, Helanshan Mountain; JXFFB, Jinxi  
 79 Fault-Fold Belt; LPM, Liupan Mountain; QLOB, Qinling Orogen Belt; THD,  
 80 Tianhuan Depression; WMTB, Western Margin Thrust Belt; WBU, Weibei Uplift;  
 81 YCB, Yinchuan Basin; YMU, Yimeng Uplift; YSS, Yishan Slope. (c) Geological map  
 82 of the central-northern section of the western margin of the Ordos Basin (modified  
 83 from Ma, 2019) and the sample locations in this study.  
 84

85 The study area is located in the central-northern section of the  
 86 western margin of the Ordos Basin (Fig. 1). Influenced by multiple

87 tectonic movements, the region has a complex evolutionary history, with  
88 several large-scale, nearly north-south-oriented faults. In general, it can  
89 be considered that the structural style of the central-northern section of  
90 the western margin of the Ordos Basin is the result of the interaction  
91 between adjacent blocks. Over the years, previous published papers  
92 investigated the structural characteristics and properties of the  
93 central-northern section of the western margin of the Ordos Basin (Yang  
94 and Zhang, 1986; Tang et al., 1988, Tang, 1992; Gan, 1990; Liu, 1995;  
95 Zhao et al., 1990), its formation mechanisms (Liu and Yang, 1997; Liu et  
96 al., 2005; Ouyang et al., 2012; Yang et al., 2011; Yang et al., 2006, 2008;  
97 Zhao, 2003; Zhao et al., 2006, 2007a, b,c), and provenance (Jiang et al.,  
98 2019). Regarding the overall exhumation process along the western  
99 margin of the Ordos Basin, previous published papers based on the  
100 apatite fission-track method suggest that the exhumation in the southern  
101 section of the western margin of the Ordos Basin began in the Middle to  
102 Late Jurassic (Chen, 1999, Chen et al., 2007; Gao et al., 2000; Zhang et  
103 al., 2000; Zhao et al., 2006, 2007a, c; Zhao, 2017; Li, 2019; Ma and He,  
104 2019; Peng Heng, 2020; Tian et al., 2023). In the central-northern section  
105 of the western margin of the Ordos Basin, low-temperature  
106 thermochronology studies are relatively scarce and have mainly focused  
107 on the Helanshan Mt. area (Ma and He, 2019; Zhao et al., 2007a; Liu,  
108 2010), the Zhuozishan Mt. region (Zhuo, 2015; Li Bin, 2006), the

Shigouyi area (Gao, 2014; Zhao et al., 2007b, c; Ma and He, 2019; Li, 2019), drilling wells such as LC1, T1, and TS1 (Ren, 1995) (Fig.2).

On the basis of the limited published thermochronological data (Ma and He, 2019; Zhao et al., 2007a, b; Liu, 2010; Zhuo, 2015; Li, 2019; Gao, 2014; Ren, 1995), it is evident that the study area recorded an exhumation event during the Mesozoic, but its timing and rate vary across different regions. The structural differences between the basin margin and the inner part have not been well clarified. Current research lacks a comprehensive perspective and does not provide a systematic understanding of tectonic events in the central-northern section of the western margin of the Ordos Basin since the Mesozoic. This greatly limits further insights into the overall tectonic evolution of the area and poses significant challenges for deeper research into intracontinental deformation in the basin and its surrounding regions.

This study applied low-temperature thermochronology methods, combined with thermal history modeling and field observation, to precisely constrain the exhumation and cooling history of the central-northern section of the western margin of the Ordos Basin. The research helps to improve our understanding of the evolution and tectonic processes in this region since the Mesozoic. Additionally, it offers a foundational reference for future oil and gas exploration efforts in the western margin of the basin.

## 2 Geological setting

The Ordos Basin, as one of the key geological element of the North China Craton, is a large basin formed during different periods and geodynamic settings (Ren et al., 2020). The evolution of the basin can be divided into several stages: Archean-Paleoproterozoic basement formation; Mesoproterozoic - Neoproterozoic rift basin development; early Palaeozoic stable continental margin sedimentation; late Palaeozoic to Middle Triassic intracratonic basin evolution; Late Triassic to Jurassic intracontinental depression basin evolution; Early Cretaceous westward contraction of the depression basin; Late Cretaceous to Cenozoic basin exhumation; formation of Cenozoic fault-depression basins in the surrounding areas (Liu et al., 2005; Ren et al., 2020; Li Tianbin, 2006).

In order to define more precisely the differences in exhumation and cooling stages since the Mesozoic era, this article further divides the research area into the ZM region, the TH region, and the MH region.

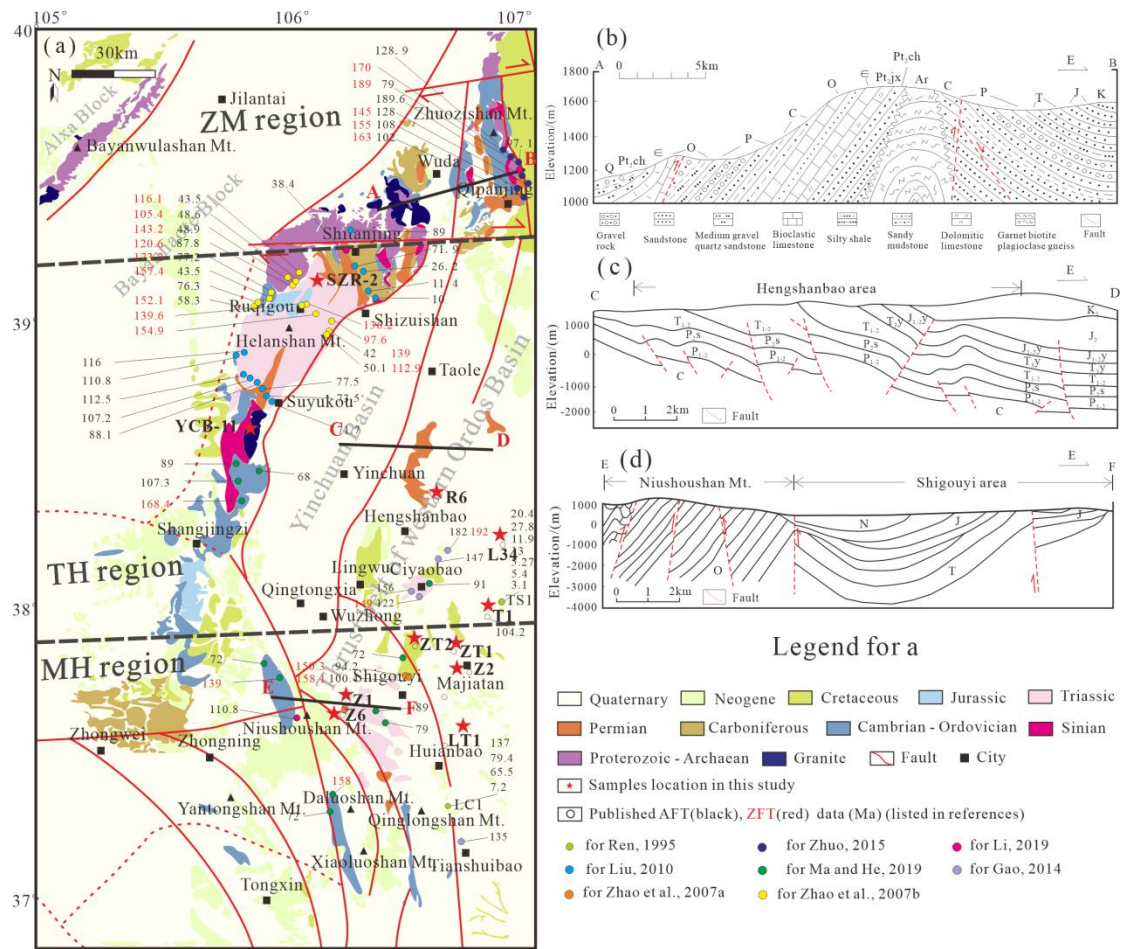


Fig. 2 (a) Compilation of previously published low-temperature thermochronological data in the study area, (b-d) W-E oriented simplified geological cross-sections (modified from Xing et al., 2024; Liu et al., 2024, and Ma and He, 2019, respectively).

In the ZM region, the main body is the Zhuozishan anticline, with an east-west length of about 20km. The core of the anticline exposes older strata, with Archean granitic gneiss of the Qianlishan Group at its core. Moving westward, it sequentially exposes the Changcheng System Huangqikou Formation, Jixian System Wangquankou Formation, Cambrian Taosigou Formation, Hulusitai Formation, Zhangxia Formation, Abuqiehai Formation, Ordovician Sandaokan Formation, Zhuozishan Formation, and the Permian Shanxi Formation and Shihezi Formation, and exposes the Carboniferous, Permian, Triassic, Jurassic, and

Cretaceous strata in sequence towards the east (Fig. 2b) (Zhuo, 2015; Xing et al., 2024). In the TH region, the faults in this area exhibit high-angle thrusting from east to west, characterized by a series of imbricated thrust faults (Fig. 2c). In the MH region, four west-dipping thrust faults develop from west to east. From west to east, the Weizhou fault zone, Qinglongshan fault zone, Shigouyi fault zone, and Yandunshan fault zone have formed in sequence. Among them, the Shigouyi fault zone, in an syncline form, is situated between the Qingshanlong Fault and the Huianbao-Shajingzi Fault (Fig. 2d).

### **3 Sampling strategy and methodology**

#### **3.1 Previous thermochronological data**

This study collected a total of 85 published low-temperature thermochronology data from the western margin of the Ordos Basin, specifically from the area between the Zhuozishan Mt. and the Tianshuibao city, including 62 apatite fission-track ages and 23 zircon fission-track ages (Fig. 3). Samples with higher mineral closure temperatures exhibit older apparent ages. The ages obtained through the apatite fission-track analysis range from 189.6 Ma to 3.1 Ma, while zircon fission-track ages range from 192 Ma to 105.4 Ma. These findings indicate a long cooling history and a complex exhumation process in the study area. Based on the collected data, we plotted histograms and kernel density estimation curves, revealing that the density peaks for apatite and

zircon are at 78 and 101 Ma, and at 153 Ma respectively (Fig.3).

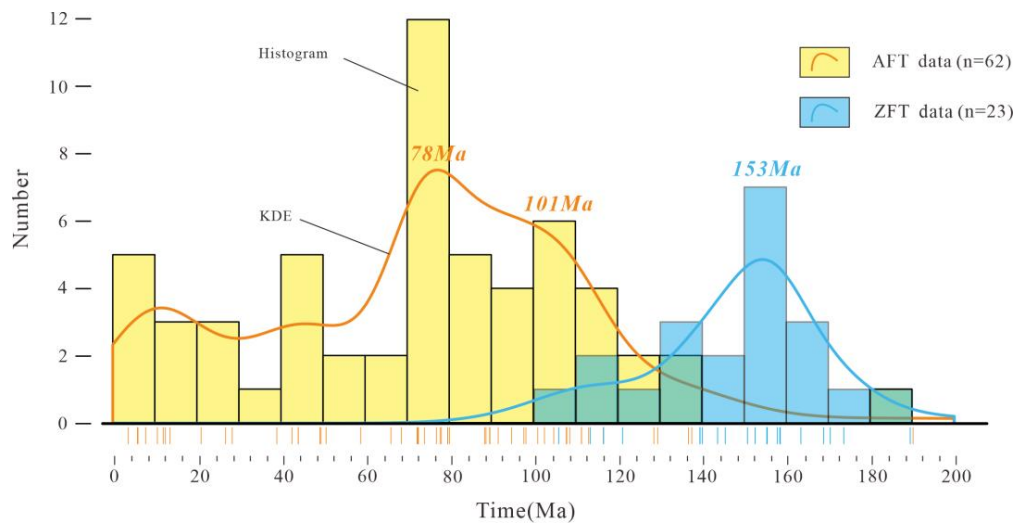


Fig.3 Histogram and kernel density estimation (KDE) plot of published thermochronological data in the study area.

In summary, previous thermochronological data indicate that multiple cooling events have occurred in the region since the Mesozoic era (Ren, 1995; Zhao et al., 2007a, b; Liu, 2010; Zhuo, 2015; Gao, 2014; Li, 2019; Ma and He, 2019). Due to the lack of thermochronological techniques such as the (U-Th)/He method and the existence of regional differences in the study area, the cooling history of the study area after the Mesozoic has not been systematically constrained.

### 3.2 Sample collection and experimental methods

This study applies low-temperature thermochronological methods to constrain the spatiotemporal evolution of the upper few kilometers of the lithosphere. Apatite fission-track analysis is sensitive to temperature variations in the range of 60 °C to 120 °C (the partial annealing zone), while apatite (U-Th)/He dating is suitable for defining the

time-temperature history in the range of 40 °C to 75 °C (Ketcham, 2005; Gallagher, 2012; Flowers et al., 2015; Farley et al., 1996).

The author has previously conducted thermochronological studies in the ZM region (Xing et al., 2024). To systematically study the differences in exhumation and cooling, the relationship between structural evolution at the basin edge and within the basin, and to address the current gaps in thermochronology in the research area, this study collected 13 valuable samples, including 11 core samples from 9 drilling wells and 2 field outcrop samples. The samples are well-distributed across the entire TH region and MH region (Fig.2a). Sample information was detailed in Table 1, and sample localities and sites were marked in Fig.1 and Fig.2.

Table 1 Sample information and summary of geochronology methods used.

Sample NO.	Formation	Lithology	Coordinate(N)	Coordinate(E)	Methods	Note
YCB-11	Ar	Granodiorite	38°25'59.9"	106°5'55.8"	AFT	TH region
SZR-2	T <sub>3</sub>	Sandstone	39°0'27.7"	106°9'15.9"	AFT	TH region
W22L34-21	P <sub>1</sub>	Sandstone	38°7'19.3"	107°6'3.2"	AFT	TH region
W22R6-6	P <sub>2</sub>	Sandstone	38°15'29.1"	106°45'50.1"	AFT	TH region
W22R6-7	P <sub>2</sub>	Sandstone	38°15'29.1"	106°45'50.1"	AFT	TH region
W22T1-5	J <sub>2</sub>	Sandstone	38°1'3.7"	107°5'9.1"	AFT	TH region
W22Z1-33	J <sub>2</sub>	Sandstone	37°40'36.2"	106°24'4.6"	AFT, AHe	MH region
W22Z1-34	J <sub>2</sub>	Sandstone	37°40'36.2"	106°24'4.6"	AFT	MH region
W22Z2-11	P <sub>2</sub>	Sandstone	37°46'51.1"	106°56'7.4"	AFT	MH region
W22ZT1-44	T <sub>3</sub>	Sandstone	37°50'37.4"	106°53'41.2"	AFT	MH region
W22ZT2-18	J <sub>2</sub>	Sandstone	37°51'53.1"	106°46'53.2"	AHe	MH region
W22Z6-16	P <sub>1</sub>	Sandstone	37°36'45.3"	106°23'14"	AFT	MH region
W22LT1-20	P <sub>1</sub>	Sandstone	37°27'8.2"	106°47'8.7"	AFT	MH region

After obtaining the samples, apatite was separated using conventional heavy liquid and magnetic separation methods. All 13 samples were analyzed using apatite fission-track (AFT) methodology.

After selecting mineral grains, the samples were prepared, tested, and analyzed at the Petroleum Thermochronology Laboratory in the Department of Geology at Northwest University. The calculation method for AFT ages follows Hasebe et al. (2004), and ages were analyzed using RadialPlotter software (Vermeesch, 2009). Additionally, the HeFTy software was utilized to simulate the cooling history (Ketcham, 2005).

Additionally, following three criteria — crystalline integrity of the automorphic particles, the purity of the particles, and ensuring that the crystal dimensions perpendicular to the c-axis exceed 60-70  $\mu\text{m}$ —apatite grains from samples Z1-33 and ZT2-18 were chosen under a high magnification (160x) binocular microscope for (U-Th)/He (AHe) dating. The dating was conducted at the Ar-Ar and (U-Th)/He Geochronology Laboratory of the Institute of Geology and Geophysics, Chinese Academy of Sciences.

Due to the complexity of annealing processes, the measured apparent ages lack any practical geological significance (Flowers et al., 2015). By utilizing the measured ages, track lengths, angle with the C-axis of mineral particles, Dpar values, this thermal history can be inversely modeled (Ketcham, 2005). In this study, HeFTy version 1.6.7 software was used for inverse modeling (Ketcham, 2005), and the Ketcham (2005) multi-dynamic annealing model was selected for the inversion simulation, along with the corrected confined track lengths. The

original confined track length was set at 16.3  $\mu\text{m}$ , and the present-day surface temperature was 20°C. The goodness-of-fit parameter (GOF) was used to indicate how well the simulation results matched the actual measurements; a higher value signifies a better fit. When the GOF value obtained from the simulation exceeds 0.05, it indicates that the simulation results are acceptable, while a GOF value greater than 0.5 indicates a very good match. The simulated ages and lengths both had GOF values greater than 0.5 and close to 1, suggesting that the simulation results closely aligned with the measured values.

## **4 Results**

### **4.1 Low-temperature thermochronology results**

#### **4.1.1 The TH region**

The AFT central ages of the two samples from well R6 (R6-6 and R6-7) are  $140.4 \pm 15.7$  Ma and  $115.3 \pm 10.2$  Ma, with average track lengths of  $11.66 \pm 1.02$   $\mu\text{m}$  and  $12.1 \pm 1.52$   $\mu\text{m}$ , respectively. The AFT central age of the sample from well L34 (L34-21) is  $130 \pm 19.8$  Ma. In the Helanshan Mt. area, the AFT central ages of samples SZR-2 and YCB-11 are  $95.2 \pm 14.8$  Ma and  $95.4 \pm 3.7$  Ma, with average track lengths of  $12.01 \pm 1.68$   $\mu\text{m}$  and  $12.88 \pm 1.11$   $\mu\text{m}$ , respectively. The AFT central ages of these five samples in this region are significantly younger than the stratigraphic ages from which they were derived, indicating that the samples have undergone annealing and cooling processes. Only the YCB-11 sample

passed the  $\chi^2$  test, with the RadialPlotter software providing a single peak age of  $95.2 \pm 3.2$  Ma. The remaining four samples did not pass the  $\chi^2$  test, suggesting that each sample contains at least two age populations. The RadialPlotter software (Vermeesch, 2009) was used to decompose the ages, and these peak ages record potential tectonic activities in this region from Late Jurassic to Eocene (Table 2, Fig. 4).

Table 2 Fission-track age obtained by the laser method

Sample	n	Ns	$\rho_s (\times 10^6/\text{cm}^2)$	$^{238}\text{U}$ ( $\times 10^{-6}$ )	Central age (Ma)	P ( $\chi^2$ ) (%)	MTL( $\mu\text{m}$ )(N)	Dpar ( $\mu\text{m}$ )
YCB-11	27	904	1.203	$26.55 \pm 8.78$	$95.4 \pm 3.7$	18	$12.88 \pm 1.11$ (97)	$1.53 \pm 0.19$
SZR-2	18	187	0.927	$20.91 \pm 1.49$	$95.2 \pm 14.8$	0	$12.01 \pm 1.68$ (43)	$1.70 \pm 0.4$
W22L34-21	7	269	1.04	$16.27 \pm 3.41$	$130 \pm 19.8$	0		$1.43 \pm 0.17$
W22R6-6	14	339	0.967	$16.38 \pm 1.8$	$140.4 \pm 15.7$	0	$11.66 \pm 1.02$ (35)	$1.66 \pm 0.23$
W22R6-7	26	852	0.946	$19.20 \pm 1.52$	$115.3 \pm 10.2$	0	$12.1 \pm 1.52$ (56)	$1.44 \pm 0.16$
W22T1-5	20	946	1.814	$47.72 \pm 4.08$	$88.3 \pm 8.3$	0	$11.3 \pm 1.22$ (78)	$1.46 \pm 0.14$
W22Z1-33	21	1066	1.547	$24.52 \pm 1.75$	$137.9 \pm 7.7$	0	$10.89 \pm 1.15$ (82)	$1.61 \pm 0.24$
W22Z1-34	15	826	2.182	$34.22 \pm 2.77$	$144.5 \pm 12.2$	0	$10.75 \pm 1.13$ (80)	$1.42 \pm 0.16$
W22Z2-11	12	502	0.794	$8.60 \pm 2.53$	$189.5 \pm 11.1$	5	$12.21 \pm 1.31$ (52)	$1.48 \pm 0.21$
W22ZT1-44	20	778	1.312	$38.34 \pm 3.7$	$71.0 \pm 8.1$	0		$1.41 \pm 0.2$
W22ZT2-18	13	643	2.416	$33.92 \pm 2.6$	$152.6 \pm 15.2$	0		$1.49 \pm 0.24$
W22Z6-16	18	398	1.092	$49.28 \pm 5.8$	$68.6 \pm 13.7$	0		$1.31 \pm 0.23$
W22LT1-20	22	677	1.135	$47.69 \pm 3.1$	$51.9 \pm 6.1$	0	$11.43 \pm 0.99$ (50)	$1.40 \pm 0.18$

Note: n: number of measured grains;  $\rho_s$  (Ns): spontaneous track densities (tracks numbers measured); P(%): probability of obtaining  $\chi^2$ -test value, a probability  $>5\%$  is indicative of a homogenous population; MTL: mean confined track lengths with c-axis correction.

283

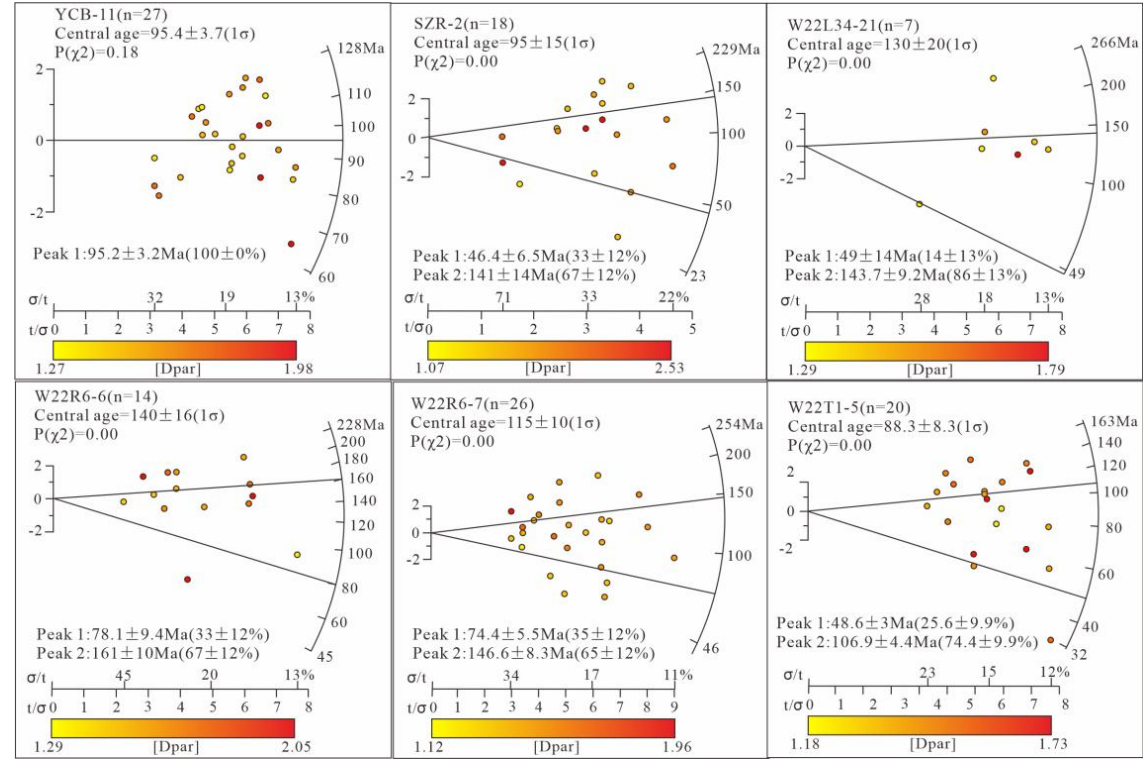
Table 3 Borehole Z1 and ZT2 apatite (U-Th)/He data.

Sample	Mass(u g)	Rs (um)	U (ppm)	Th (ppm)	Th /U	[eU] (ppm)	mol 4He	Std. mol 4He	FT	Cor Age (Ma)	± σ (Ma)
W22Z1-							3.0575	3.7211E	0.7		
33-A1	3.00	47.2	33.7	35.4	1.1	42.1	E-14	-16	09	63.48	3.38
W22Z1-							3.9018	4.8104E	0.7		
33-A2	5.95	64.3	20.9	9.0	0.4	23.1	E-14	-16	88	67.06	3.58
W22Z1-							4.0084	8.5601E	0.7		
33-A3	2.48	47.8	41.7	114.7	2.8	68.7	E-14	-16	07	61.64	3.43
W22ZT							7.6887	9.0770E	0.7		
2-18-A1	3.95	53.6	8.4	3.7	0.5	9.2	E-15	-17	46	52.61	2.82
W22ZT							4.2928	5.2774E	0.6		
2-18-A2	2.69	47.0	45.7	160.9	3.6	83.5	E-14	-16	98	50.69	2.66
W22ZT							1.2764	1.5287E	0.7		
2-18-A3	2.91	48.4	19.0	4.3	0.2	20.1	E-14	-16	23	56.31	3.17

284

Note:Rs, equivalent spherical radius; eU, effective uranium concentration; FT, α-ejection correction factor; Cor. Age, AHe age with α-ejection correction.

285



286

287

Fig.4 AFT age Radial plots for The TH region

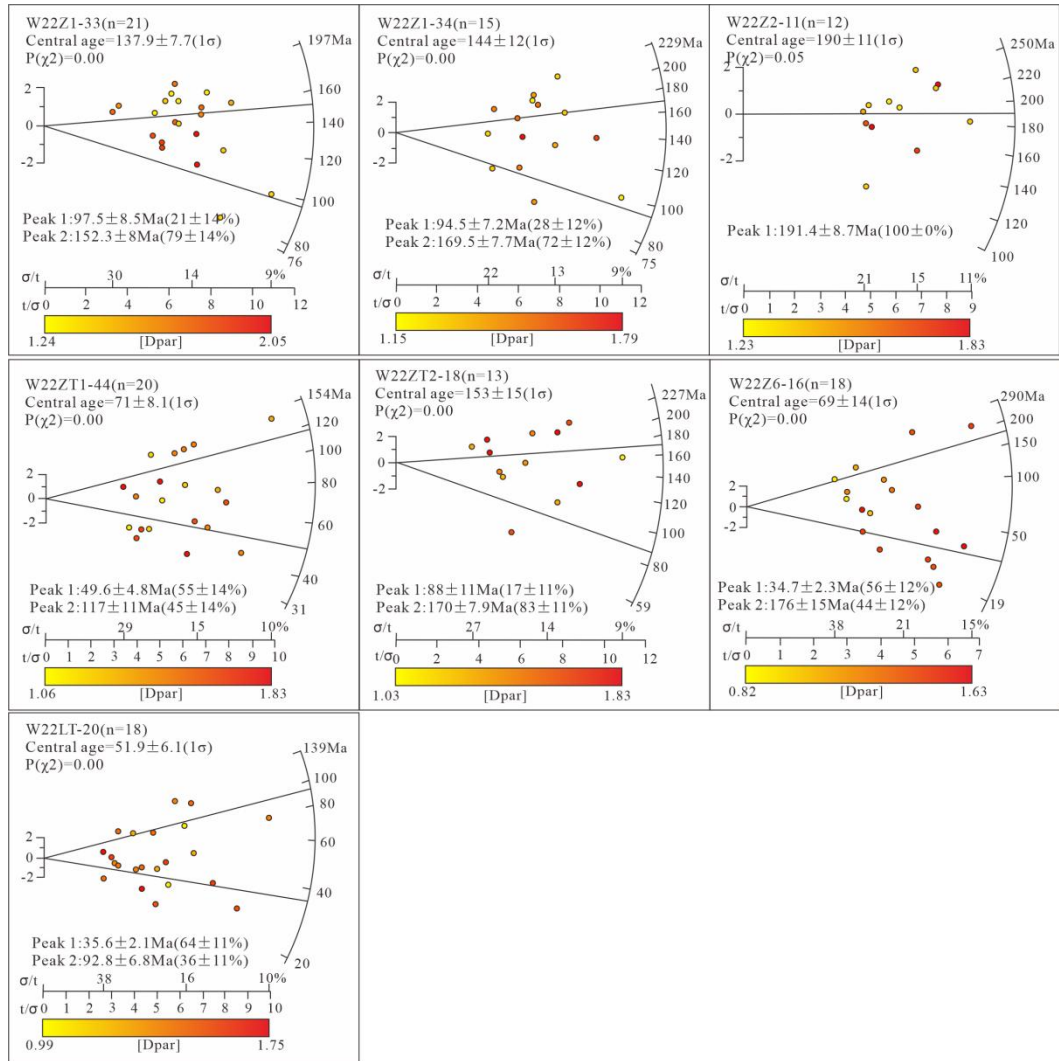


Fig.5 AFT age Radial plots for The MH region

#### 4.1.2 The MH region

Due to this region being a key area for oil and gas exploration, a large number of drilling samples are available. Except for sample Z2-11, which passed the  $\chi^2$  test, the remaining samples did not pass the test. The fission-track ages obtained for this region range from 189.5 Ma to 35.6 Ma and were statistically divided into three peak values: 42 Ma, 95 Ma, and 170 Ma (Fig.5). All of these ages are significantly younger than the stratigraphic ages, indicating that they have undergone exhumation and

cooling processes. The three single-grain AHe ages for sample Z1-33 range from 61.64 Ma to 67.06 Ma, while the three single-grain AHe ages for sample ZT2-18 range from 50.69 Ma to 56.31 Ma, with no significant correlation to eU, recording late exhumation and cooling events (Table 3, Fig. 6).

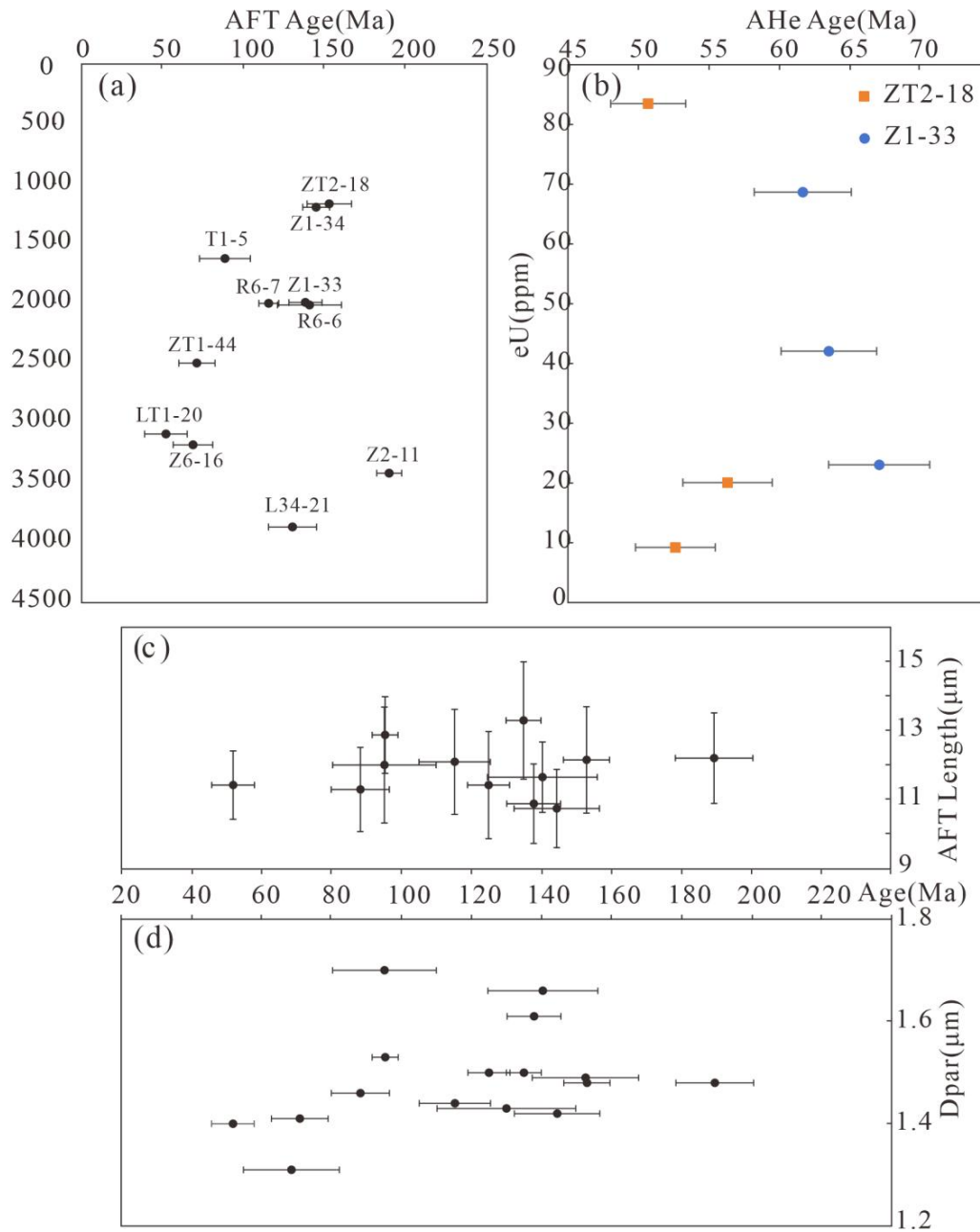


Fig.6 (a) Relationships between AFT Age and depth; (b) Relationships between AHe age and eU; (c), Relationships between AFT Age and AFT length; (d) Relationships between AFT Age and Dpar.

In addition, the correlation between track length and AFT age indicates a complex cooling history in the region. Considering the different annealing dynamics (Ketcham et al., 2007), the chemical composition of the grains may influence the AFT age and length (Carlson et al., 1999; Barbarand et al., 2003). However, the  $D_{par}$  values in the samples range from 1.31  $\mu\text{m}$  to 1.70  $\mu\text{m}$ , showing minimal variation and no significant correlation with the AFT ages. This suggests that the influence of chemical composition on AFT age is either minimal or nonexistent.

#### **4.2. Thermal history modeling**

Among the 13 samples, 12 with more extensive length information were selected for thermal history simulation, representing a broad distribution across the study area to assess their potential thermal history and determine their exhumation and cooling times. The goodness-of-fit parameters for both length and age in this simulation were above 0.90, indicating a good fit. The inverted time-temperature paths are shown in Fig. 7.

The modeling results indicate significant differences in the thermal histories of samples from different regions. Two samples from the western part of the TH region record a rapid exhumation event from 110 Ma to 90 Ma, followed by a long period of slow cooling, and finally a rapid cooling event around 25 Ma. The R6 well records a rapid cooling

history during the Late Cretaceous (ca. 155 Ma). The T1 well records a rapid exhumation event from 95 Ma to 85 Ma. In the MH region, the Z1 well simulation reveals rapid exhumation from 158 Ma to 137 Ma, and the three samples in this region show rapid exhumation between 70 Ma and 50 Ma (Fig.7).

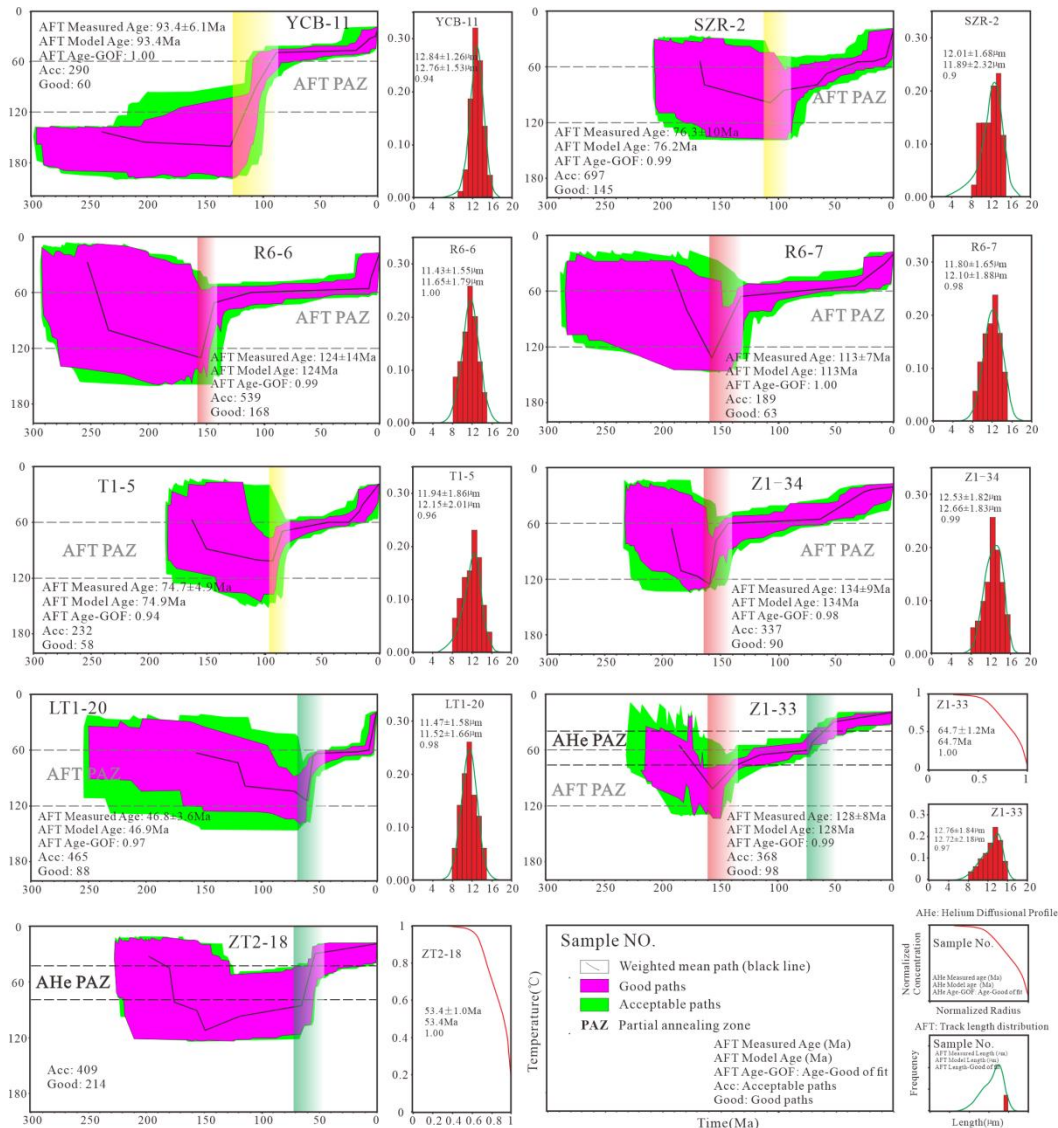


Fig.7 Thermal history inverse modeling calculated by HeFTy (Ketcham, 2005), using the model of Ketcham et al. (2007) and Flowers et al. (2009). HeFTy modeling tests possible  $t - T$  curves by using the Monte-Carlo inverse modeling approach. Shaded parts of different colors represent different cooling periods.

## 5 Discussion

From the thermal history simulation paths, the exhumation initiation

times generally fall in the late Jurassic; however, there are still differences. The exhumation of the TH region was later, while the other region was earlier, which is related to the tectonic evolution and stress of their respective locations. Additionally, the exhumation intensity varies from east to west across the regions. For example, the samples from the MH region indicate that exhumation occurred earlier in the western samples compared to those in the eastern side. These observations are closely linked to the reverse thrusting and imbrication along the western margin (Fig. 8).

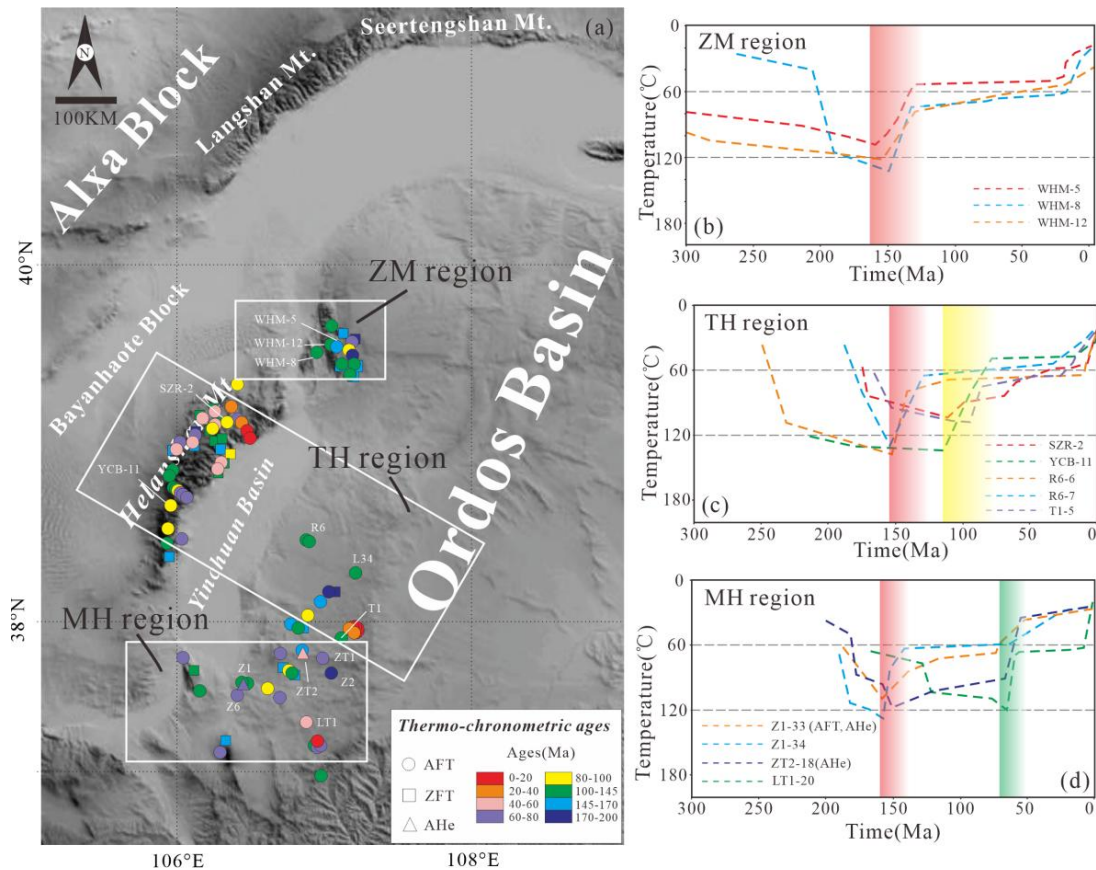


Fig.8 (a) Summary of all available thermochronology data. The data sources are the same as in Fig. 2. (b-d), The thermal history paths summarized in this study are from the ZM region, TH region, and MH region, respectively.

## **5.1 Exhumation Process Differences and Geological Responses in the central-northern section of the western margin of the Ordos Basin Constrained by Low-Temperature Thermochronology**

### **5.1.1 The ZM region**

Based on the test results, the exhumation rate of this area can be calculated. The calculation formula is:

$$U = (\theta - T_0) / K \times F \quad (1)$$

Here, U represents the exhumation rate (the exhumation rate of apatite since it entered the annealing zone), measured in m/Ma;  $\theta$  is the closure temperature of the mineral, in °C; K is the geothermal gradient, in °C/100m;  $T_0$  is the mean annual surface temperature, in °C; and F represents the fission-track age, in Ma. For the sake of discussion and comparison, this paper adopts the same parameters as Zhao Hongge (2007c), with K set at 4 °C/100m,  $T_0$  at 25 °C, and  $\theta$  at 110 °C.

The author also conducted thermochronology work in the ZM region this year and inverted its exhumation history and thermal history, indicate that the region underwent three major exhumation stages since the Mesozoic: Late Jurassic (160 Ma-150 Ma), this phase marks the first major exhumation stage in the area, with an average exhumation rate of ca. 45 m/Ma and an average cooling rate of ca. 2 °C /Ma. This exhumation corresponds to the early stages of the Yanshanian orogeny in the region, triggering reverse thrusting and imbrication, as evidenced by

the inversion results of all three samples; Early Cretaceous - Oligocene (130 Ma - 30 Ma), this stage represents a period of slow cooling, with an average exhumation rate of ca. 10 m/Ma and an average cooling rate of ca. 1 °C/Ma, suggesting the absence of significant tectonic events during this time. The timing and exhumation differences among the samples during this phase may reflect the varying effects of different episodes of the Yanshanian orogeny (stages II, III, and IV) on the region; Cenozoic (since ca. 30 Ma), The most recent exhumation stage is associated with the Himalayan orogeny, which caused further significant exhumation in the region, with an average exhumation rate of ca. 30 m/Ma and an average cooling rate of ca. 1.2 °C/Ma.

#### **5.1.2 The TH region**

In the Taole-Hengshanbao part, two samples from well R6 have peak ages of 161 Ma, 146 Ma, 78 Ma, and 74 Ma, suggesting possible tectonic events during the Late Jurassic and Late Cretaceous. The thermal history models of both samples show similar results, indicating three phases of exhumation: Late Jurassic (155 Ma-145 Ma), a period of significant exhumation begins, with an average exhumation rate of ca. 48 m/Ma and an average cooling rate of ca. 2.4 °C/Ma; Early Cretaceous - Oligocene (145 Ma-30 Ma), this phase is characterized by slow exhumation, with an average exhumation rate of ca. 7.5 m/Ma and an average cooling rate of ca. 0.3 °C/Ma; Cenozoic (ca. 30 Ma-present), a period of intense and

rapid exhumation occurs, with an average exhumation rate of ca. 25 m/Ma and an average cooling rate of ca. 1 °C/Ma. The ages recorded in samples R6-6 and R6-7 are basically the same. The slight differences in their AFT model results arise because R6-6 was located deeper, meaning it exited the partial annealing zone later than R6-7 during exhumation. This caused the AFT age constraints for R6-6 to be slightly younger. For the T1-5 sample, located in the THD, exhumation began at the end of the Early Cretaceous, with an average exhumation rate of ca. 50 m/Ma and an average cooling rate of ca. 2 °C/Ma. This area previously had a complete sedimentary sequence and extensive sediment distribution, forming the thick Tianhuan syncline in the Ordos Basin (Zhao et al., 2007a).

The exhumation in this area is related to the exhumation in the neighboring Helanshan Mountain region and the intense faulting and subsidence in the Yinchuan Graben. The thermal history models of the two Helanshan Mountain samples (SZR-2 and YCB-11) also have a certain pattern in spatial and temporal distribution: The YCB-11 sample in the south entered a rapid cooling stage from the end of the Early Cretaceous to the Late Cretaceous (130 Ma-95 Ma), with an average exhumation rate of ca. 46 m/Ma and an average cooling rate of ca. 1.8 °C/Ma, followed by slow cooling with an average exhumation rate of ca. 2.5 m/Ma until the Eocene (~35 Ma), after which it rapidly exhumation to the surface, with an average exhumation rate of ca. 18 m/Ma and an average

cooling rate of ca. 0.7 °C /Ma. The northern SZR-2 sample, however, shows a delayed cooling history at essentially the same rate of exhumation, with cooling events occurring primarily after the Early Cretaceous. The exhumation pattern, with earlier exhumation in the south and later exhumation in the north, aligns with previous studies on the Helanshan Mountain region (Ma and He, 2019).

### 5.1.3 The MH region

In the southern, Majiatan-Huianbao part, two samples from well Z1 (Z1-33 and Z1-34) indicate that exhumation in the well began during the Late Jurassic (ca. 160 Ma). Combined AFT and AHe inversion results show that sample Z1-33 experienced rapid exhumation between 158 Ma and 137 Ma, with an average exhumation rate of ca. 45 m/Ma and an average cooling rate of ca. 1.8 °C /Ma, followed by slower exhumation from 137 Ma to 110 Ma, with an average exhumation rate of ca. 13 m/Ma and an average cooling rate of ca. 0.52 °C /Ma, and then entered another phase of intense exhumation between 70 Ma and 50 Ma, with an average exhumation rate of ca. 37.5 m/Ma and an average cooling rate of ca. 1.5 °C /Ma. Sample Z1-34, constrained only by AFT data, shows large-scale exhumation starting from 160 Ma to 140 Ma, a slow exhumation phase from 140 Ma to 64 Ma, and then a rapid exhumation event. Since the temperature at 64 Ma is beyond the AFT-sensitive temperature range, the thermal history model of well Z1, especially for

the later stages of exhumation and cooling, is more reliably constrained by the dual-dating sample Z1-33. The AFT simulation of sample LT1-20 reveals an exhumation event between 60 Ma and 55 Ma, with an average exhumation rate of ca. 60 m/Ma and an average cooling rate of ca. 4 °C /Ma, and the AHe thermal history simulation of sample ZT2-18 similarly shows an exhumation event from 62 Ma to 52 Ma, with an average exhumation rate of ca. 65 m/Ma and an average cooling rate of ca. 6.5 °C /Ma. This indicates an early Cenozoic tectonic cooling event in the region.

## **5.2 Transformation of the Meso-Cenozoic Tectonic Regime and Regional Dynamic Background in the North-Central Western Margin**

At the end of the Paleoproterozoic, the Ordos Block formed and merged with the North China Craton. Following this, under an extensional tectonic environment, large-scale rifting occurred, creating northeast-trending rift troughs with some structural inheritance from the basement, which was covered by strata from different periods, including strata of the Proterozoic, Paleozoic, Mesozoic, and Cenozoic eras (Bao et al., 2019; Wang et al., 2019). In the early Palaeozoic, the Ordos region transitioned into a stable cratonic basin. During multiple marine transgressions and regressions, a set of widespread marine carbonate sediments, interbedded with clastic rocks, was deposited across the region.

The large-scale Caledonian orogeny caused a depositional hiatus between Ordovician and Carboniferous strata, resulting in an unconformable contact between the two. Since the late Palaeozoic, the Ordos Basin has begun the transition from sea-land intersection to terrestrial sedimentation, and the development of the North China marginal sea - coastal shallow sea sedimentary. During the Late Triassic to Early Cretaceous, the basin saw intracratonic fluvial-lacustrine sedimentation. Since the Late Cretaceous, the basin has entered a phase of overall exhumation and peripheral subsidence. From the late Mesozoic, the Ordos Basin became an independent sedimentary basin. Its sedimentary evolution has been primarily influenced by the Mesozoic-Cenozoic tectonic systems, undergoing multiple sedimentary cycles and exhumation-related transformations (Fig. 9).

In the Triassic period, influenced by the Indosinian Orogeny, the Qinling-Qilian ancient ocean basin finally closed. The mountains collided and continued to compress, resulting in sedimentary hiatuses or erosion. Therefore, the Late Triassic and Early Jurassic strata were in parallel unconformable contact (Zhang et al., 2001). The Indosinian tectonic stress originated from the collision and docking of the South China Plate and the North China Plate during the Triassic period, resulting in a north-south stress field (Peng, et al., 2024).

The Yanshanian orogeny was the primary tectonic deformation

487 period for the Ordos Basin, with the particularly intense compression  
488 deformation and exhumation erosion in the Late Jurassic. These  
489 movements caused the Jurassic and underlying sedimentary layers to  
490 become involved in widespread deformation, resulting in a clear angular  
491 unconformity with the overlying strata. This deformation was especially  
492 pronounced along the western margin of the basin, where much of the  
493 surface deformation that is observed today had already taken shape  
494 during this period (Darby and Ritts, 2002). The tectonic stress of the  
495 Yanshanian orogeny originated from the Tethys tectonic domain,  
496 eastward compression of the Alxa block, westward subduction of the  
497 Pacific plate, and closure of the Okhotsk Ocean.

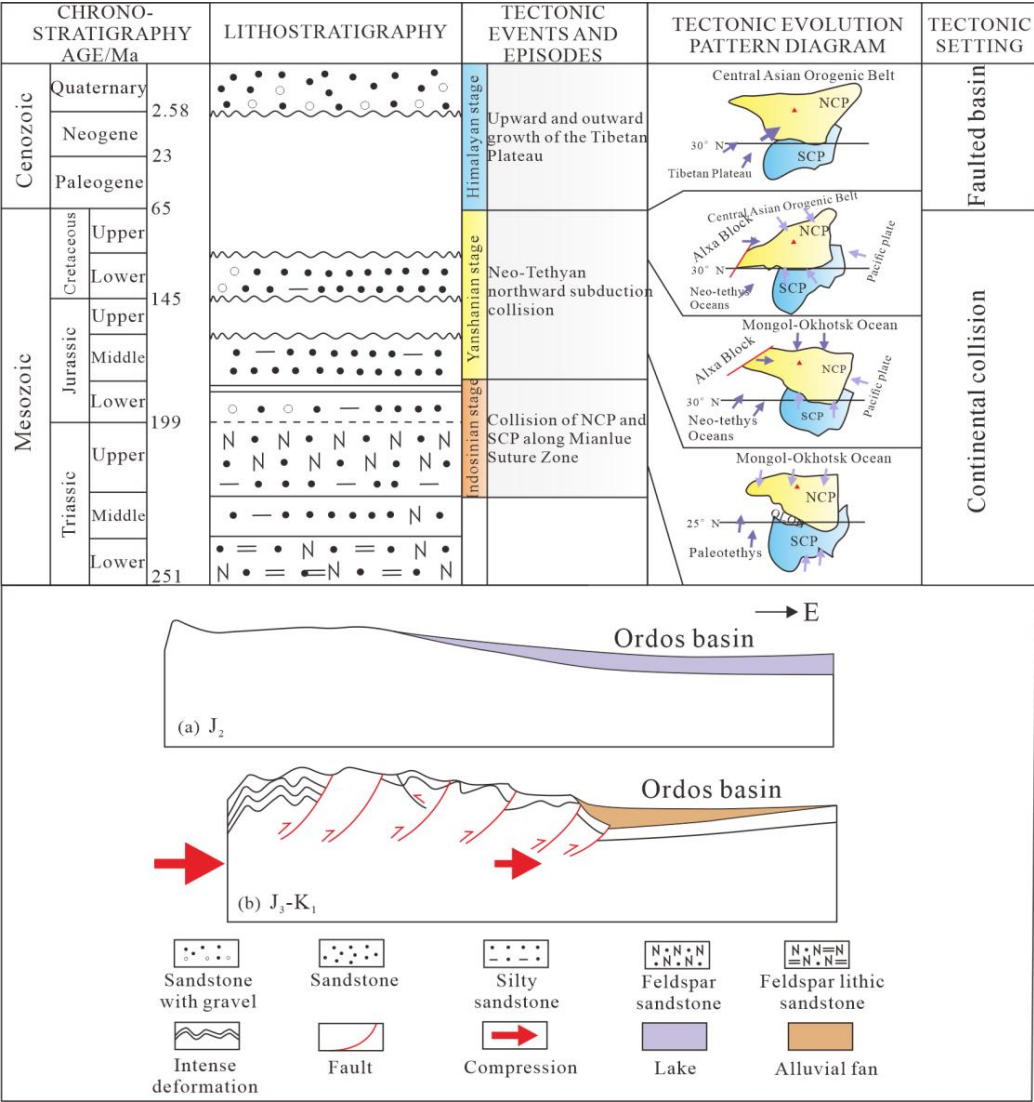


Fig.9 Dynamic model diagram of the northern part of the western margin of Ordos Basin.(Modified from Zhang et al., 2021; Peng et al., 2022)

In the Late Jurassic, the Yanshanian orogeny triggered the first major large-scale exhumation in the study area. During this period, the compressional forces that were primarily north-south oriented during the earlier Indosinian orogeny transitioned to an east-west orientation characteristic of the Yanshanian phase (Dong et al., 2007, 2008, 2021; Zhang et al., 2008). This tectonic exhumation event aligns with the peak ages obtained from fission-track at 170 Ma, 161 Ma, and 153 Ma. The tectonic evolution of this phase was controlled by several factors, notably

the southwest Tethys tectonic domain, eastward compression from the Alxa Block, and the closure of the Okhotsk Ocean in the north during the Late Jurassic (Zhao et al., 2023). Additionally, far-field effects from the subduction of the Pacific Plate played a role (Darby and Ritts, 2002, 2007; Faure et al., 2012; Liu, 1998; Yang et al., 2008; Zhang et al., 2020, 2021, 2022; Zhao et al., 2023). Previous paleomagnetic studies revealed that the Ordos Basin was undergoing a counterclockwise rotation during this period (Zhao and Coe 1987; Zhang et al., 2000). These regional tectonic processes collectively shaped the large-scale exhumation and deformation seen during this period, marking a significant phase in the area's geological history. The comprehensive analysis of stress fields in the Late Jurassic indicates that multiple tectonic blocks around the Ordos Basin experienced subduction, collision, compression, and even mutual rotation. These interactions led to the folding and exhumation of Jurassic strata, accompanied by a series of imbricate thrust faults pushing from west to east (Zhao and Coe, 1987; Ma and He, 2019; Zhang et al., 2021, 2022). In the ZM region, the collision with the Alxa Block initiated significant exhumation, while in the MH region, the overall exhumation of the Qilian Mountains and its thrusting into the basin resulted in strong thrusting structures. This contributed to the earlier onset of exhumation in areas like ZM region and MH region. The compressional deformation shows a general pattern of stronger exhumation and deformation in the west and at

the margins, with weaker effects in the interior of the basin.

The Early Cretaceous was a crucial period in the evolution of the Ordos Basin, the deep thermal material in the basin began to upwell. Northern China was under an extensional tectonic regime, linked to the broader lithospheric thinning and basin development of the North China Craton during this time (Ren et al., 2007, 2008, 2014, 2017, 2020, 2022). In the central Taole region, extensional faults from this period are observable in seismic profiles (Zhao et al., 2007a). Towards the end of the Early Cretaceous, the regional tectonic stress field reversed due to the multiple phases of the Yanshanian orogeny (phases II, III, IV). The area was simultaneously influenced by the northward collision of the Yangtze Plate and the far-field effects of the Pacific Plate. The northern region was affected by the closure of the Okhotsk Ocean, and the western region continued to experience direct compression from the eastward movement of the Alxa Block (Yang et al., 2008; Zhang et al., 2020, 2022; Zhao et al., 2023). The previously deposited strata experienced intensified folding and exhumation under compressional stress. This led to the formation of large-scale south-north-oriented thrust faults and imbricate thrust structures. At this point, the tectonic landscape of the study area is basically formed.

During the Cenozoic, the tectonic deformation of the Ordos Basin was primarily driven by the collision between the Indian and Eurasian

plates. This is the primary cause of the closure of the Tethys Ocean and one of the responsible for the stresses applied in the region, with significant tectonic activity occurring during the Eocene to Miocene. The continued Himalayan orogeny caused strong tectonic movements in the region, leading to further exhumation of the strata. The strata predominantly displaying parallel and angular unconformities. This tectonic activity has significantly shaped the present-day landscape. The neighboring Alxa region, located at the northeastern edge of the Tibetan Plateau, was affected by the plateau's Cenozoic exhumation. Its deformation is closely linked to the evolution of the Tibetan Plateau (Zhang et al., 2023; Rao et al., 2016; Lei et al., 2022). Concurrently, the Pacific Plate continued its northwestward subduction during this period. Numerous geochronological records document the exhumation and northeastward expansion of the northeastern Tibetan Plateau during the Cenozoic, particularly in the Eocene and Miocene (England and Housemann, 1986; Wang et al., 2008; Lease et al., 2011, 2012; Craddock et al., 2011; Ding et al., 2022; Peng et al., 2019; Zhao et al., 2023; Zhang et al., 2020). Low-temperature thermochronology data, along with thermal history reconstructions constrained by AHe and AFT, reveal rapid exhumation during the Eocene to Miocene, likely a result of the far-field effects of the Cenozoic exhumation of the northeastern Tibetan Plateau and the northwestward subduction of the Pacific Plate.

Overall, the study area has undergone the Indosinian, Yanshanian, and Himalayan orogenies since the Mesozoic era. In the central-northern section of the western margin of the basin, especially during the Yanshanian period, the Alxa rigid block sandwiched between the South China and North China plates is squeezed out in a southeast direction, directly affecting the Helanshan Mountains and the northern part of the western margin of the basin, causing the stress direction to shift towards a nearly east-west direction.

## **6 Conclusion**

(1) This study used apatite fission-track (AFT) and apatite (U-Th)/He (AHe) dating methods, combined with thermal history modeling, to precisely constrain the exhumation and cooling history of the central-northern sections of the western margin of the Ordos Basin. The analysis reveals significant differences in the timing and intensity of exhumation across different regions: ZM region experienced a large-scale exhumation during the Late Jurassic (160-150 Ma), slow exhumation at Early Cretaceous - Oligocene (130 Ma-30 Ma), and severe exhumation after Oligocene (30 Ma-); TH region began at Late Jurassic - Early Cretaceous (155 Ma-145 Ma), slowly exhumation at Early Cretaceous - Oligocene (145 Ma-30 Ma), and then violently exhumation; MH region experienced a significant exhumation at Late Jurassic - Early Cretaceous (158 Ma-137 Ma), with a slightly slower exhumation rate at 137 Ma-110

Ma, and entered a severe exhumation stage again at Late Cretaceous - Eocene (70 Ma-50 Ma). Overall, the northern and southern sections began earlier, while the central section initiated exhumation slightly later. These findings highlight the spatial variation in exhumation timing and rates within the western Ordos Basin.

(2) The study reveals that the Yanshanian orogeny had the most significant tectonic impact on the study area. Multiple exhumation events during the Mesozoic are responses to the multi-phase Yanshanian orogeny in this region. Since the Cenozoic, rapid exhumation influenced by the Himalayan orogeny has shaped the current landscape.

#### **Author Contributions**

**Xing Guangyuan:** writing original draft, conceptualization, methodology, writing review editing, software, resources, data curation, formal analysis.

**Ren Zhanli:** writing original draft, conceptualization, methodology, investigation, resources, writing - review and editing, supervision, project administration, funding acquisition. **Qi Kai:** writing original draft, writing review editing. **Guo Sasa:** investigation. **Liu Yanzhao:** investigation.

**Zhang Ying :** methodology, **Lan Huaping:** methodology.

#### **Competing interests**

The contact author has declared that none of the authors has any competing interests.

#### **Data Availability Statement**

The data that support the findings of this study are available from the corresponding author upon reasonable request.

## **Acknowledgements**

Financial support for this study were jointly provided by the Major Projects of PetroChina Changqing Oilfield Company (ZDZX2021) and PetroChina Changqing Oilfield Company Science and technology Major Projects "Research on Tectonic-Sedimentary Environment, Hydrocarbon Accumulation Conditions and Favorable Exploration Zones in the Deep Strata of Ordos Basin" (2024D1JC06). Our heartfelt gratitude is given to those anonymous reviewers for their scientific and linguistic revisions to the manuscript.

## **Conferences**

- [1] Bao Hongping, Shao Dongbo, Hao Songli, Zhang Guisong Ruan Zhengzhong Liu gang and Ouyang Zhengjian. Basement Structure and Early Sedimentary Cover Evolution of the Ordos Basin[J]. Earth Science Frontiers, 2019, 26(1): 33-43.
- [2] Barbarand J, Carter A, Wood I and Hurford T. Compositional and structural control of fission-track annealing in apatite[J]. Chemical Geology, 2003, 198(1-2): 107-137.
- [3] Carlson W D, Donelick R A, Ketcham R A. Variability of apatite fission-track annealing kinetics: I. Experimental results[J]. American mineralogist, 1999, 84(9): 1213-1223.
- [4] Chen Gang, Wang Zhiwei, Bai Guojun, Sun Jianbo, Zhang Huiruo and Li Xiangdong. Peak Age Events and Their Sedimentary-Tectonic Responses in the Mesozoic-Cenozoic Ordos Basin[J]. Geology in China, 2007(03): 375-383.
- [5] Chen Gang. Composition of Mesozoic Terrigenous Clastic Rocks and Their Tectonic Attributes in the Ordos Basin[J]. Acta Sedimentologica Sinica, 1999(03): 409-413.
- [6] Craddock W, Kirby E, Zhang H P. Late Miocene-Pliocene range growth in the interior of the northeastern Tibetan Plateau, Lithosphere, 2011, 3(6):420-438.
- [7] Darby B J, Ritts B D. Mesozoic contractional deformation in the middle of the Asian tectonic collage: the intraplate Western Ordos fold-thrust belt, China[J]. Earth and Planetary Science Letters, 2002, 205(1-2): 13-24.

- [8] Darby B J, Ritts B D. Mesozoic structural architecture of the Lang Shan, North-Central China: Intraplate contraction, extension, and synorogenic sedimentation[J]. *Journal of Structural Geology*, 2007, 29(12): 2006-2016.
- [9] Ding L, Kapp P, Cai F, Garzione C N, Xiong Z Y, Wang H Q and Wang C. Timing and mechanisms of Tibetan Plateau uplift[J]. *Nature Reviews Earth & Environment*, 2022, 3(10): 652-667.
- [10] Dong Shuwen, Zhang Yueqiao, Chen Xuanhua, Long Changxing, Wang Tao Yang Zhenyu and Hu Jianmin Formation and Deformation Characteristics of the Late Jurassic Multidirectional Convergent Tectonic System in East Asia[J]. *Acta Geoscientia Sinica*, 2008, 29(3): 306-317.
- [11] Dong Shuwen, Zhang Yueqiao, Long Changxing, Yang Zhenyu, Ji Qiang, Wang Tao, Hu Jianmin and Chen Xuanhua. New Interpretations of the Jurassic Tectonic Transformations and the Yanshan Movement in China[J]. *Acta Geologica Sinica*, 2007, 81(11): 1449-1461.
- [12] Dong Yunpeng, Li Wei, Zhang Feifei, Sun Jiaopeng and He Dengfeng. Formation and Evolution of the Helan Mountain in the Northern Section of the North-South Tectonic Belt[J]. *Journal of Northwest University (Natural Science Edition)*, 2021, 51(6): 951-968
- [13] England P and Houseman G. Finite strain calculations of continental deformation: Comparison with the India-Asia Collision Zone. *Journal of Geophysical Research: Solid Earth*, 1986, (B3):3664-3676.
- [14] Farley K A, Wolf R A, Silver L T. The effects of long alpha-stopping distances on (U-Th)/He ages[J]. *Geochimica et cosmochimica acta*, 1996, 60(21): 4223-4229.
- [15] Faure M, Lin W, Chen Y. Is the Jurassic (Yanshanian) intraplate tectonics of North China due to westward indentation of the North China block?[J]. *Terra Nova*, 2012, 24(6): 456-466.
- [16] Flowers R M, Farley K A, Ketcham R A. A reporting protocol for thermochronologic modeling illustrated with data from the Grand Canyon[J]. *Earth and Planetary Science Letters*, 2015, 432: 425-435.
- [17] Gallagher K. Transdimensional inverse thermal history modeling for quantitative thermochronology[J]. *Journal of Geophysical Research: Solid Earth*, 2012, 117(B2).
- [18] Gan Kewen. On the Genesis Mechanism of Thrust Belts and Hydrocarbon Prospects of the Western Margin of the Ordos Basin[J]. In: Yang Junjie. *Thrust Tectonics and Hydrocarbon in the Western Ordos Basin*. Lanzhou: Gansu Science and Technology Press, 1990, 31239.
- [19] Gao Feng, Wang Yuejun, Liu Shunsheng, Hu Baoqing. Study on the Thermal History of the Western Margin of the Ordos Basin Using Apatite Fission Track Analysis[J]. *Geotectonica et Metallogenia*, 2000(01): 87-91.
- [20] Gao Shaohua. Mesozoic-Cenozoic Evolutionary Modification of the Lateral Structural Belt in the Central Western Ordos Basin and Its Significance for Oil and Gas[D]. Xi'an: Northwest University, 2014.
- [21] Hasebe N, Barbarand J, Jarvis K, Carter A and Hurford A J. Apatite fission-track chronometry using laser ablation ICP-MS[J]. *Chemical Geology*, 2004, 207(3-4): 135-145.

- [22] Jiang Suyang, Huang Wenhui, Zhang Yongsheng, Xing Enyuan, Gui Baoling, Peng Yuan, Zhao Haitong and Shang Wenjuan. Tectonic Setting and Provenance Analysis of the Sandstones from the Sandaokan Formation in the Northern Segment of the Western Ordos Basin[J]. Journal of Northeast Petroleum University, 2019, 43(4): 17-28.
- [23] Ketcham R A, Carter A, Donelick R A, Barbarand J. and Hurford A J. Improved modeling of fission-track annealing in apatite[J]. American Mineralogist, 2007, 92(5-6): 799-810.
- [24] Ketcham R A. Forward and inverse modeling of low-temperature thermochronometry data[J]. Reviews in mineralogy and geochemistry, 2005, 58(1): 275-314.
- [25] Lease R O, Burbank D W, Hough B, Wang Z C and Yuan Daoyang. Pulsed Miocene growth in northeastern Tibet: insights from Xunhua Basin magnetostratigraphy and provenance. GSA Bull., 2012, 124(5-6): 657-677.
- [26] Lease R O, Burbank D W, Clark M K, Farley K A, Zheng D W and Zhang Huiping. Middle Miocene reorganization of deformation along the northeastern Tibetan Plateau, Geology, 2011, 39(4): 359-362.
- [27] Lei Qiyun, Yu Jingxing, Zhang Peizhen, Zheng Wenjun, Zhang Zhuqi, Du Peng and Wang Yin. Tectonic geomorphology and prehistoric earthquakes of the West Helanshan fault, West Ordos, and its implications for regional tectonics and seismic hazard[J]. Tectonophysics, 2022, 833: 229375.
- [28] Li Bin. Study on the Thrust Belt Structure and Hydrocarbon Controlling Factors in the Western Ordos Basin[D]. Northwest University, 2019.
- [29] Li Bin. Tectonic Characteristics and Hydrocarbon Accumulation Studies of the Foreland Basin in the Western Ordos Basin[D]. Graduate School of the Chinese Academy of Sciences (Guangzhou Institute of Geochemistry), 2006.
- [30] Li Tianbin. Characteristics and Evolution of Thrust Structures in the Western Ordos Basin[D]. China University of Geosciences (Beijing), 2006.
- [31] Liu Chiyang, Zhao Hongge, Wang Feng, and Chen Hong. Mesozoic Tectonic Characteristics of the Western Margin of the Ordos Basin[J]. Acta Geologica Sinica, 2005, 79(6): 737-747.
- [32] Liu Chiyang, Huang Lei, Zhao Hongge, Wang Jianqiang, Yang Lihua, Xi Xiaodong and Peng Heng. Continental lateral transformation structures and their geological effects[J]. Acta Geologica Sinica, 2024, 98(12): 3455-3477.
- [33] Liu Hefu. Types of Foreland Basins and Styles of Fold-Thrust Structures[J]. Earth Science Frontiers, 1995, 2(3): 59-68.
- [34] Liu Jianhui. Cenozoic Extensional Uplift of the Helan Mountains and Qinling Mountains and Analysis of Fault Frictional Heating Using Apatite Fission Track Method[J]. International Seismological Dynamics, 2010(3): 31-33.
- [35] Liu S F, The coupling mechanism of basin and orogen in the western ordos Basin and adjacent regions of China[J]. Journal of Asian Earth Science, 1998, 16(4): 369-383.
- [36] Liu Shaofeng and Yang Shigong. North-South Differences and Their Formation Mechanism on the Western Margin of the Ordos Basin[J]. Geological Science, 1997,

32(3): 397-408.

[37] Ma Jinghui, He Dengfa. Mesozoic-Cenozoic Tectonic Events in the Helan Mountain Tectonic Belt and Adjacent Areas: Constraints from Unconformities and Fission Track Analysis[J]. *Acta Petrologica Sinica*, 2019, 35(4): 1121-1142.

[38] Ouyang Zhengjian, Chen Hongde, Feng Juanping. Tectonic Characteristics and Evolution of the Central and Southern Segments of the Western Margin of the Ordos Basin[J]. *Modern Geology*, 2012, 26(04): 691-695.

[39] Peng Heng, Wang Jianqiang, Liu Chiyang, Zhang Shuohua, Zattin Massimiliano, Wu Nan and Feng Qi. Thermochronological constraints on the Meso-Cenozoic tectonic evolution of the Haiyuan-Liupanshan region, northeastern Tibetan Plateau[J]. *Journal of Asian earth sciences*, 2019, 183(Oct.1):103966.1-103966.13.

[40] Peng Heng, Wang Jianqiang, Liu Chiyang, Huang Lei, Zattin Massimiliano. Mesozoic exhumation and ca. 10 Ma reactivation of the southern Yin Shan, North China, revealed by low-temperature thermochronology[J]. *Tectonophysics*, 2022, 823: 229189.

[41] Peng Heng. Fission Track Thermochronology Analysis and Its Geological Significance in the Southwestern Adjacent Area of the Ordos Block[D]. Northwest University, 2020.

[42] Peng Heng, Ding Lin, Liu Chiyang, Zattin Massimiliano and Wang Licheng. Middle Triassic transcontinental connection between the North China Craton and the Paleo-Tethys Ocean. *Commun Earth Environ*, 2024, 5, 775.

[43] Rao Gao, Chen Peng, Hu Jianmin, Yu Yangli and Qiu Jianhua. Timing of Holocene paleo-earthquakes along the Langshan Piedmont Fault in the western Hetao Graben, North China: Implications for seismic risk[J]. *Tectonophysics*, 2016, 677: 115-124.

[44] Ren Zhanli, Cui Junping, Qi Kai, Yang Peng, Liu Xinshe, Zhang Caili, Yang Guilin, Gao Yanfang, Zhang Ying and Xing Guangyuan. New Advances in the Theoretical Research and Methods for Restoring the Thermal Evolution History of Deep and Ultra-deep Layers in Overlapping Basins[J]. *Journal of Northwest University (Natural Science Edition)*, 2022, 52(6): 910-929.

[45] Ren Zhanli, Liu Li, Cui Junping, Xiao Hui and Gao Shengli. Application of Tectonic Thermal Evolution History in the Study of Hydrocarbon Accumulation Phases[J]. *Oil & Gas Geology*, 2008, 29(4): 502-506.

[46] Ren Zhanli, Qi Kai, Liu Runchuan, Cui Junping, Chen Zhipeng, Zhang Yuanyuan, Yang Guilin and Ma Qian. The Dynamical Background of Early Cretaceous Tectonic Thermal Events in the Ordos Basin and Their Control on the Accumulation Periods of Various Minerals, Including Oil and Gas[J]. *Acta Petrologica Sinica*, 2020, 36(4): 1213-1234.

[47] Ren Zhanli, Tian Tao, Li Jinbu, Wang Jiping, Cui Junping, Li Hao, Tang Jianyun and Guo Ke. Research Methods for Thermal Evolution History of Sedimentary Basins and Progress in Reconstructing Thermal Evolution History of Overlapping Basins[J]. *Journal of Earth Sciences and Environment*, 2014, 36(3): 1-20.

[48] Ren Zhanli, Yu Qiang, Cui Junping, Qi Kai, Chen Zhanjun, Cao Zhanpeng, Yang Peng. Thermal Evolution History of the Ordos Basin and Its Control on

Hydrocarbons[J]. *Earth Science Frontiers*, 2017, 24(03): 137-148.

[49] Ren Zhanli, Zhang Sheng, Gao Shengli, Cui Junping, Xiao Yuanyuan, Xiao Hui. Tectonic Thermal Evolution History of the Ordos Basin and Its Significance for Accumulation and Mineralization[J]. *Science in China: Series D, Earth Sciences*, 2007(S1): 23-32.

[50] Ren Zhanli. Study on the Geothermal History of the Ordos Basin Using the Apatite Fission Track Method[J]. *Chinese Journal of Geophysics*, 1995, 38(03): 339-349..

[51] Tang Xiyuan, Guo Zhongming, Wang Dingyi. Characteristics, Evolution, and Hydrocarbon Exploration of the Thrust Nappe Structure Belt in the Western Ordos Basin[J]. *Oil & Gas Geology*, 1988, 9(1): 1-10.

[52] Tang Xiyuan. Thrust Nappe Structures and Hydrocarbon Exploration on the Western Margin of the Shaanxi-Gansu-Ningxia Basin[M]. Xi'an: Northwest University Press, 1992.

[53] Tian Chaoyang, Chen Hong, Liu Xinshe, Gong Wangbin, Zhao Weibo and Kang Rui. Fission Track Ages and Mesozoic Tectonic Uplift in the Niushou Mountain—Luoshan Area of the Western Ordos[J]. *Journal of Geological Mechanics*, 2023, 29(05): 599-617.

[54] Vermeesch P. RadialPlotter: A Java application for fission track, luminescence and other radial plots[J]. *Radiation Measurements*, 2009, 44(4): 409-410.

[55] Wang C S, Zhao X X, Liu Z F, Lippert P C, Graham S A, Coe R S, Yi H S, Zhu L D, Liu Shun and Li Y L. Constraints on the early uplift history of the Tibetan Plateau, *Proc. Natl. Acad. Sci. USA*, 2008, 105(13): 4987-4992.

[56] Xing Guangyuan, Ren Zhanli, Qi Kai, Guo Sasa and Liu Yanzhao. Low-Temperature Thermochronologic Analysis and Geologic Significance of the Northern Part of the Western Margin of the Ordos Basin: A Case Study of the Moergou Profile in the Zhuozishan Area, Inner Mongolia, China[J]. *Geological Journal*, 2024. <https://doi.org/10.1002/gj.5108>.

[57] Yang Hua, Fu Jinhua, Ouyang Zhengjian, Sun Liuyi. Analysis of Tectonic-Sedimentary Environments during the Late Triassic in the Western Margin of the Ordos Basin[J]. *Acta Sedimentologica Sinica*, 2011, 29(03): 427-439.

[58] Yang Junjie and Zhang Borong. Strike-Slip Rift and Associated Thrust Belt: A Case Study of the Yinchuan Graben and Hengshanpu Thrust Belt[J]. *Petroleum Exploration and Development*, 1986(02): 1-8.

[59] Yang Shengbin, Geng Xinxia, Guo Qingyin, Hou Guiting and Liu Zhongbao. Mesozoic Tectonic Evolution of the Northern Segment of the Western Ordos Basin[J]. *Geological Review*, 2008, 54(3): 307-315.

[60] Yang Shengbin, Guo Qingyin, Hou Guiting and Sun Hua. Subsidence History and Sedimentary Response in the Northern Segment of the Western Ordos Basin[J]. *Journal of Peking University: Natural Science Edition*, 2006, 42(2): 192-198.

[61] Zhai Mingguo. The Formation, Evolution, and Metallogenesis of the North China Craton[J]. *Mineral Deposits*, 2010 (1): 24-36.

[62] Zhai Mingguo. The Ordos Block: The Key to Unraveling the Mysteries of Early Continental Formation, Evolution, and Tectonic Regime of the North China Craton[J].

- Chinese Science Bulletin, 2021, 66(26): 3441-3461.
- [63] Zhang Chengli, Gou Longlong, Diwu Chunrong, Liu Xinyu, Zhaojiao and Hu Yuhua. Precambrian Geological Events, Nature, and Geological Significance of the Basement in the Western North China Craton[J]. *Acta Petrologica Sinica*, 2018, 34(4): 981-998.
- [64] Zhang Guowei, Dong Yunpeng, Yao Anping. A New Starting Point for the Study of Orogenic Belts and Orogenesis[J]. *Northwest Geology*, 2001, 34(1): 1-9.
- [65] Zhang Jin, Cunningham D, Qu Junfeng, Zhang Beihang, Li Jinyi, Zhao Heng, Niu Pengfei, Hui Jie Yun Long, Zhao Shuo, Zheng Rongguo and Zhang Yiping. Poly-phase structural evolution of the northeastern Alxa Block, China: Constraining the Paleozoic-Recent history of the southern central Asian Orogenic belt[J]. *Gondwana Research*, 2022, 105: 25-50.
- [66] Zhang Jin, Wang Yannan, Qu Junfeng, Zhang Beihan, Zhao Heng and Yun Long. Mesozoic intracontinental deformation of the Alxa Block in the middle part of Central Asian Orogenic Belt: A review[J]. *International Geology Review*, 2021, 63(12): 1490-1520.
- [67] Zhang Jin, Yun Long, Zhang Beihang, Qu Junfeng, Zhao Heng, Hui Jie, Wang Yannan and Zhang Yiping. Deformation at the easternmost Altyn Tagh Fault: Constraints on the growth of the northern Qinghai-Tibetan plateau[J]. *Acta Geologica Sinica-English Edition*, 2020, 94(4): 988-1006.
- [68] Zhang Jin., Ma Jinzong and Ren Wenjun. Mechanism of North-South Differences in the Overthrust Belt on the Western Margin of the Ordos Basin[J]. *Geotectonica et Metallogenia*, 2000(02): 124-133.
- [69] Zhang Jiasheng, He Zixin, Fei Anqi, Li Tianbin and Huang Xiongnan. Large Margin Thrust Nappe System in the Northern Segment of the Western Ordos Basin[J]. *Geological Science*, 2008, 43(2): 251-281.
- [70] Zhang Jin, Zhang Beihang, Zhao Heng, Yun Long, Qu Junfeng, Wang Zhenyi, Yang Yaqi and Zhao Shuo. Characteristics and Mechanisms of Late Cenozoic Deformation in the Beishan-Alashan Region[J]. *Earth Science Frontiers*, 2023, 30(5): 334.
- [71] Zhao Zhongyuan, Liu Chiyang, Ren Zhanli. Geology of Oil and Gas Basins and System Engineering in Their Research[J]. *Oil & Gas Geology*, 1990, 11(1): 108-113.
- [72] Zhao Hongge, Liu Chiyang, Wang Feng, et al. Tectonic Partitioning and Characteristics of the Western Margin of the Ordos Basin[J]. *Oil & Gas Geology*, 2006, 27(2): 173-179.
- [73] Zhao Hongge, Liu Chiyang, Wang Feng, et al. Uplift Timing and Evolution of the Helan Mountains[J]. *Science in China: Series D*, 2007a, 37(A01): 185-192.
- [74] Zhao Hongge, Liu Chiyang, Wang Jianqiang, et al. Exploration of Tectonic Attributes during the Late Triassic in the Western Ordos Basin[J]. *Geological Journal of China*, 2007b, 34(3): 384-391.
- [75] Zhao Hongge, Liu Chiyang, Yao Yaming, Wang Feng, Yin Yan. Fission Track Evidence of Differential Uplift in the Western Ordos Basin[J]. *Journal of Northwest University (Natural Science Edition)*, 2007c, (03): 470-474.
- [76] Zhao Hongge. Tectonic Characteristics and Evolution of the Western Ordos

Basin[D]. Northwest University, 2003.

[77] Zhao Pan, Xu Bei, Chen Yan. Mongolian–Okhotsk Ocean: Evolutionary Process and Final Closure[J]. *Science in China: Earth Sciences*, 2023, 53(11): 2541-2559.

[78] Zhao X, Coe R S. Palaeomagnetic constraints on the collision and rotation of North and South China. *Nature*, 1987, 327:41-144.

[79] Zhao Xiaochen. Mesozoic Tectonic Evolution and Later Modification of the Northern Section of the North-South Tectonic Belt in China[D]. Xi'an: Northwest University, 2017.

[80] Wang Wei, Zhao Yue, Liu Xiaochun, Hu Jianmin, Wei Chunjing, Xiao Wenjiao, Du Jinxue, Wang Shilin and zhanliqing. Metamorphism of diverse basement gneisses of the Ordos Basin: Record of multistage Paleoproterozoic orogenesis and constraints on the evolution of the western North China Craton[J]. *Precambrian Research*, 2019, 328: 48-63.

[81] Zhuo Yuzhou. Determination of Mesozoic-Cenozoic Uplift Events in the Zhuozishan Area of the Northwestern Ordos Basin and Their Tectonic Significance[D]. Northwest University, 2015.